Journal of Biomolecular NMR, 2 (1992) 597–618
ESCOM

J-Bio NMR 089

Complete sequence-specific ^{1}H NMR resonance assignment of hyperfine-shifted residues in the active site of a paramagnetic protein: Application to *Aplysia* cyano-metmyoglobin

Jun Qin and Gerd N. La Mar*

Department of Chemistry, University of California, Davis, CA 95616, U.S.A.

Received 15 June 1992
Accepted 11 September 1992

Keywords: *Aplysia* myoglobin; Hyperfine shift; Paramagnetic relaxation; 2D NMR; Sequence-specific assignment

SUMMARY

Two-dimensional sequence-specific ^{1}H NMR resonance assignment methodology (Wüthrich, 1986) has been applied for the first time to a 18-kDa paramagnetic hemoprotein (cyano-met *Aplysia* Mb) to identify all the hyperfine-shifted residues. The assignment was greatly facilitated by the fact that hyperfine shifts of residues impart a strong temperature dependence to the cross peaks, which aids location and identification, and provides improved spectral dispersion, particularly in the fingerprint region. 2D COSY and TOCSY were found to be surprisingly effective in locating the complete spin connectivities of all of the hyperfine-shifted residues, with the exception of the axially coordinated His^{95} imidazole ring, whose proton resonances were found to exhibit severe line broadening (> 400 Hz). Conventional 1D NOE and NOESY with short mixing times, combined with paramagnetic-induced relaxation effects, led to the successful assignment of even extremely broad proton signals. Three helical stretches and two loop regions were identified as the source of all hyperfine-shifted residues: the F helical residues 3–9, the E-helix residues 6–14, the G-helix residues 5–9, the FG-loop residues 1–4 and the CD-loop residues 1–4. These segments comprise all the residues that make contact with the heme and modulate the reactivity of the prosthetic group. The sequence-specific identifications of the active-site residues revealed that the solution structure of *Aplysia* metMbCN is fully consistent with that observed by X-ray diffraction in single crystals for a variety of other derivatives, except for the distal Arg^{66} (E10), which is turned into the heme pocket, as found only in the metMbF crystal structure (Bolognesi et al., 1990). The ready identification, by their temperature sensitivity, and the complete assignments of all hyperfine-shifted residues of *Aplysia* metMbCN demonstrate that sequence-specific assignment can be profitably applied to paramagnetic proteins, and that it should be possible to determine the solution structures of paramagnetic proteins, at least for low-spin complexes, by using NMR techniques used for diamagnetic proteins.

* To whom the correspondence should be addressed.

Abbreviations: Mb, myoglobin; NMR, nuclear magentic resonance; metMb, metmyoglobin (ferric); 2D, two dimensional; 1D, one dimensional; COSY, two-dimensional correlated spectroscopy; MCOSY, conventional magnitude two-dimensional correlated spectroscopy; TOCSY, two-dimensional total correlation spectroscopy; NOE, nuclear Overhauser Effect; NOESY, two-dimensional nuclear Overhauser effect spectroscopy; ppm, parts per million.

INTRODUCTION

The solution-structure determination of a diamagnetic protein by using ^{1}H NMR spectroscopy relies on the sequence-specific assignment of all amino acid residues (Wüthrich, 1986; Clore and Gronenborn, 1987). This procedure involves identification of the spin-coupling networks, including the backbone $C^{\alpha}H$:NH, of the individual residues in a bond correlation experiment, followed by sequential placement of these residues along the backbone, using characteristic dipolar connectivities provided by NOESY experiments. Spectral congestion tends to limit 2D ^{1}H NMR approaches to proteins of $\sim$100 residues; larger proteins generally require isotopic labeling ($^{13}C/^{15}N$) of amino acids for use with 2D and/or higher dimensional NMR methods (Clore and Gronenborn, 1989, 1991; Wagner, 1990). For paramagnetic metalloproteins, the unpaired electron spins of the metal ions lead to line broadening and enhanced spin-lattice relaxation, especially for active-site reisudes that can obscure spin coupling and undermine the development of NOEs (Ernst et al., 1987; Neuhaus and Williamson, 1989). Indeed, 2D ^{1}H NMR sequence-specific assignments in paramagnetic proteins to date have been restricted to the main chain and side chains remote from the metal center of proteins of maximally $\sim$100 residues (Feng et al., 1989).

The unique and valuable information provided by a ^{1}H NMR spectrum of a paramagnetic protein, however, resides primarily in the active-site residues that experience hyperfine shifts (Satterlee, 1985; Emerson and La Mar, 1990b), and many such proteins are large by current 2D NMR standards (Emerson and La Mar, 1990a; de Ropp and La Mar, 1991). A particularly important subclass of paramagnetic metalloproteins are the low-spin ferric hemoproteins, as represented by ferricytochromes *c* (Feng et al., 1989) and *b* (McLachlan et al., 1988; Wu et al., 1991), and the cyano complexes of ferric myoglobin, Mb (Emerson and La Mar, 1990a), hemoglobin, Hb (Peyton et al., 1988; Sylvia and La Mar, unpublished results), and heme peroxidases (Thanabal et al., 1987; Thanabal and La Mar, 1989; Dugad et al., 1990; de Ropp and La Mar, 1991). These proteins range in size from 12 kDa to over 100 kDa. Most of these proteins display ^{1}H NMR spectra for which the hyperfine-shifted active-site signals are very sensitive to the genetic origin of the protein, and several of the proteins are very sensitive to synthetic point mutation (Satterlee, 1985; Rajarathnam et al., 1992). Understanding of the functional properties of these proteins requires the assignment of the hyperfine-shifted residues and detailed molecular structural determination of the active site.

Recently, we demonstrated that the majority of the active-site side-chain residues of sperm whale metMbCN ($\sim$17 kDa) could be assigned by using 2D ^{1}H NMR methods, where extensive reliance was placed on the availability of a crystal structure to interpret NOESY data (Emerson and La Mar, 1990a). Subsequently, we showed that the bond connectivity of most of the side chains could be detected in spite of linewidths up to $\sim$100 Hz (Yu et al., 1990). It was noted that while paramagnetic relaxation rendered the 2D-bond correlation experiments less effective than with a diamagnetic protein, the unique temperature dependence of the hyperfine shifts for active-site residues compensated for this by providing increased spectral resolution and a method for differentiating cross peaks involving active-site residues from those remote from the metal center. In order to put the solution structure determination of paramagnetic proteins on a basis comparable to that of diamagnetic proteins, it is clearly necessary to investigate the feasibility of carrying out sequence-specific assignments, particularly for the active site. For this purpose, we selected a 146-residue ($\sim$18 kDa) myoglobin from the sea hare, *Aplysia limacina*, which we investigated in the

S = 1/2 metMbCN state. This Mb lacks the conserved distal His of mammalian systems (replaced by Val) (Tentori et al., 1973) and can unfold reversibly under a variety of conditions in solution (Brunori et al., 1972). Hence, it serves as a prototype for characterized Mbs for elucidation of the detailed distal control of ligand binding to the iron (Wittenberg et al., 1965; Antonini and Brunori, 1971; Brunori et al., 1986) and of the nature of protein folding (Giacometti et al., 1979; Janes et al., 1987). Moreover, X-ray crystal structures of three paramagnetic forms, unligated metMb, metMbF, and metMbN_3, exhibit important differences with regard to the structure of the distal pocket (Bolognesi et al., 1989, 1990; Mattevi et al., 1991). Hence, not only does this protein serve as an important test case for sequence-specific assignment strategies but the results of such assignments should shed light on the structure of the active site.

Our goal was to develop a strategy for sequentially assigning the residues in the heme pocket of *Aplysia* metMbCN, whose relaxation rates and chemical shifts are influenced by the paramagnetism of the low-spin iron. Our emphasis on hyperfine-shifted paramagnetically relaxed residues has two bases. Firstly, residues inconsequentially influenced by paramagnetism can be studied by conventional 2D and/or higher dimensional NMR methodology and are of no interest in this report. Hence, we targeted the residues for which any proton exhibits a significant hyperfine shift; other residues or portions thereof (backbone) were assigned only when necessary to effect the sequence-specific assignment of the target residue. Secondly, an additional goal of the study was not only to assign the paramagnetically influenced residues, but to do so in a manner that can be used for proteins larger than those normally studied by 2D NMR. In order to achieve these goals, we focused on the temperature sensitivity of peak positions detected in a 2D experiment. Since hyperfine-shifted resonances exhibit a characteristic inverse (Curie) temperature dependence (Emerson and La Mar, 1990b), the variable temperature characteristic uniquely identifies such resonances. Problems anticipated in a 2D sequence-specific assignment in a paramagnetic protein include missing bond correlation cross peaks due to broad lines, weak NOESY cross peaks due to short T_1, and the absence of the usual diamagnetic chemical-shift correlation that is important for defining the functionality of a proton set.

Our strategy for effecting sequence-specific assignments was to: (1) identify all hyperfine-shifted (temperature-sensitive) resonances which exhibit COSY cross peaks in ^2H_2O, and use COSY and TOCSY to locate all remaining protons for each spin-coupling network which can identify the residues; (2) search for additional hyperfine-shifted temperature-sensitive proton signals which exhibit only NOESY cross peaks (or 1D NOEs) in ^2H_2O; (3) connect the spin systems for the hyperfine-shifted residues to the backbone with COSY and TOCSY in ^1H_2O solution to locate the NHs (fingerprint region); and (4) utilize NOESY in ^1H_2O to locate sequentially the residues with hyperfine-shifted protons. As a convenient standard for strongly hyperfine-shifted peaks, we set a lower limit for the slope of a plot of shift versus reciprocal temperature at $|1.1| \times 10^3$ ppm · K for non-exchangeable protons. For labile protons which exhibit some temperature sensitivity even in diamagnetic systems, we set a lower limit for the slope at $|1.3| \times 10^3$ ppm · K. Protons with such slopes have been shown to exhibit > 1.5 ppm hyperfine shifts in sperm whale metMbCN (Emerson and La Mar, 1990b; Rajarathnam et al., 1992).

Specific questions we addressed are: (1) Can *all* hyperfine-shifted signals be efficiently located by their temperature sensitivity?; (2) How effective are 2D methods for locating the complete spin-systems of such signals?; (3) Can hyperfine-shifted residues be assigned by sequential backbone NOEs?; (4) Do the located residues account for all of the heme cavity side chains expected on the

basis of the Mb fold?; and (5) How well does the NOESY cross-peak pattern and paramagnetic-induced relaxivity reflect the qualitative structural features of the crystal structures of the various *Aplysia* Mb-derivatives?

EXPERIMENTAL PROCEDURES

Sample preparation

The native *Aplysia* Mb used was the same sample described in detail previously (Peyton et al., 1989). The sample concentrations were ~ 3 mM in ^2H_2O and ~ 4 mM in ^1H_2O at pH 8.9 and 5.3.

^1H NMR measurements

All ^1H NMR experiments were carried out in a GE Omega 500 MHz spectrometer. The 1D NOE spectra, SUPERWEFT spectra, and the nonselective spin-lattice paramagentic relaxation times for the resolved peaks were obtained as described previously (Emerson and La Mar, 1990a). For phase-sensitive TOCSY (Braunschweiler and Ernst, 1983; Bax and Davis, 1985; Davis and Bax, 1985), NOESY (States et al., 1982), and conventional n-type COSY (MCOSY) (Bax et al., 1981; Bax, 1984), the method described by States et al. (1982) was used to provide quadrature detection in the t1 dimension. The MLEV-17 mixing scheme (Bax and Davis, 1985) was used in the TOCSY experiments, and the MLEV-17 pulse was written in such a way that the magnetization was aligned along the effective axis of rotation of the 180° composite pulse to obtain optimal sensitivity (Rance, 1987). Solvent suppression, when required, was achieved by direct saturation in the relaxation delay period. Blocks (512) were collected with two different spectral widths for all the 2D experiments (15 500 Hz to cover all the proton resonances and 8000 Hz to emphasize the amino acid resonances for better resolution). Scans (96–512) were accumulated for each block with a free induction decay of 2048 complex data points. The 90°-pulse width was 21 μs for TOCSY and 13 μs for the other 2D experiments. Thirty-two dummy scans were used, and two repetition rates were used for all 2D experiments: 3 s^{-1} to emphasize broad cross peaks (512 scans per block), and 0.7 s^{-1} to emphasize weakly relaxed cross peaks (96 scans per block).

NMR data processing

Datasets were processed on a Silicon Graphics work station, using FELIX software. Phase-sensitive NOESY and TOCSY were processed with 30°-shifted sine-bell-squared apodization in both dimensions. MCOSY data were processed with an unshifted sine-bell-squared apodization in both dimensions. The apodization function over different complex points in t1 and t2 dimensions was used: apodization over 256, 512, 1024 points to emphasize fast-relaxing broad cross peaks at the expense of resolution; apodization over 2048 points to emphasize slowly relaxing cross peaks. All 2D spectra were zero-filled to 2048 points in the t1 dimension, with a final data size of 2048 × 2048 points.

RESULTS

Location of strongly hyperfine-shifted resonances

The resolved portions of the 500-MHz ^1H NMR spectrum for *Aplysia* metMbCN in ^1H_2O and ^2H_2O at 25 °C are illustrated in Figs. 1A and 1B, respectively. Some 31 nonlabile proton resonan-

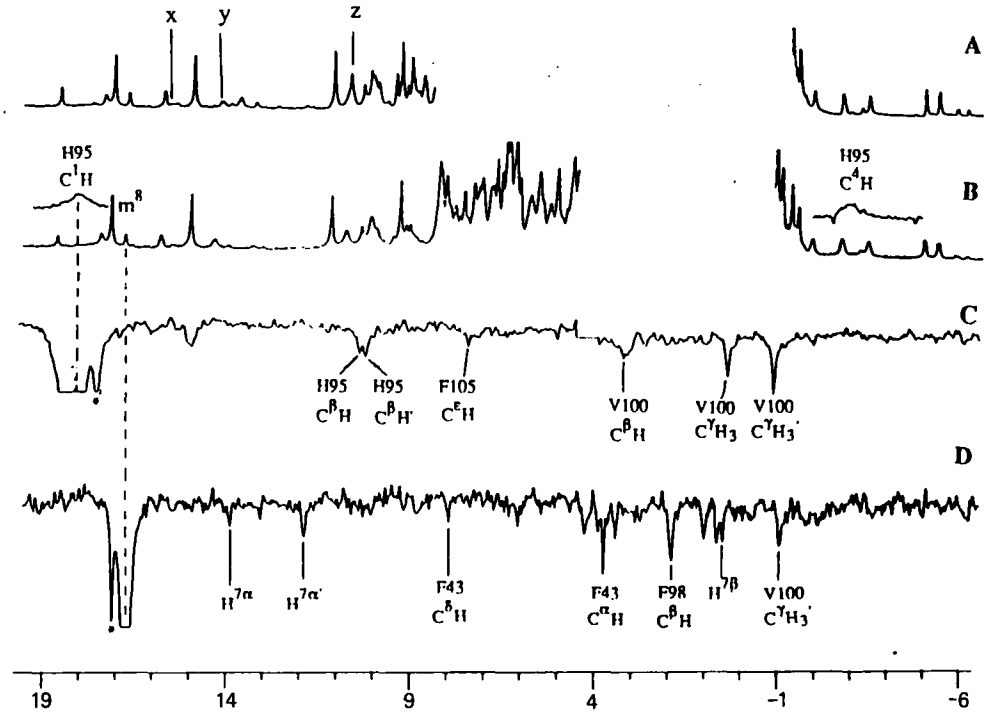

Fig. 1. Hyperfine-shifted portions of the 500-MHz ^{1}H NMR spectra of *Aplysia* metMbCN, pH 8.9. (A) In ^1H_2O, 25 °C, repetition rate $1s^{-1}$. Three resolved labile protons are labeled x, y, z. (B) In ^2H_2O, 25 °C, the repetition rate was $1s^{-1}$. The inset indicates two broad signals revealed by ID SUPERWEFT spectra collected at a $15\text{-}s^{-1}$ repetition rate. (C) In ^2H_2O, 25 °C, the 1D steady-state NOE difference spectrum upon irradiation of the low-field broad His^{95} C^{4}H signal is shown in the inset of Fig. 1B. The NOEs are all assigned and labeled (see text). (D) In ^2H_2O, 25 °C, the 1D steady-state NOE difference spectrum upon irradiation of the minor heme 8-CH_3. The NOE pattern to amino acids is the same as that for irradiation of the major heme 5-CH_3 (Peyton et al., 1989). The peaks labeled with * were due to off resonance effects.

ces could be resolved outside the 0–8 ppm range at some temperatures (Fig. 1B); three additional labile proton signals (labeled x, y, and z in Fig. 1A) were resolved in the low-field region. The protein exhibited a dynamic equilibrium between two forms, with an interconversion rate of $1.85 \times 10^{-4}\ s^{-1}$ (Bellelli et al., 1987), and an equilibrium has been proposed to involve alternate orientations of the heme about the α, γ-meso axis in a ratio of 5:1 (Peyton et al., 1989). In this report we emphasize complete assignments of the hyperfine-shifted resonances solely in the major form; limited assignments in the minor form are also considered. A nonselective T_1 determination of the resolved resonances yielded T_1 values for strongly relaxed protons as listed in Tables 1 and 2. Two very broad ($\sim$ 400 Hz) signals, which must have been from the imidazole ring of the axial His^{95}, are emphasized in a SUPERWEFT trace, as illustrated in the inset of Fig. 1B (Peyton et al., 1989; Emerson and La Mar, 1990a).

Magnitude COSY spectra with a repetition rate $3\ s^{-1}$ in ^2H_2O in 10° intervals over the temperature range 25 to 45 °C located 38 strongly temperature-sensitive resonances (slope $> |1.1| \times 10^3$ ppm · K) involved in 35 cross peaks in ^2H_2O. These signals are labeled with an asterisk and their

TABLE 1
^{1}H NMR SPECTRAL PARAMETERS FOR HEME RESONANCES

Heme peaks	Spin system[a]	δ_{Obs}[b] (ppm)	Slope[c] ($\times 10^3$)	T_1[d] ($\times 10$) (ms)
1-CH_3		11.78	1.4*	17
3-CH_3		17.80 (19.34)	4.9*	14
5-CH_3		15.61 (9.64)	0.9*,[e]	15
8-CH_3		9.95 (17.44)	−1.3*	27
2-H^{α}		16.42 (13.94)	2.5*	18
2-$H^{\beta c}$	1	−4.39 (−5.59)	8.8*	16
2-$H^{\beta t}$		−4.78 (−5.30)	−4.8*	19
4-H^{α}		5.17 (4.89)	−3.1*	
4-$H^{\beta c}$	2	−0.63 (−1.20)	−3.1*	16
4-$H^{\beta t}$		−0.48 (−0.85)	−1.8*	17
6-H^{α}		18.05 (4.13)	−1.8*	15
6-$H^{\alpha'}$		14.93 (4.53)	7.1*	14
6-H^{β}	3	−1.34 (−2.65)	10.5*	18
6-$H^{\beta'}$		1.57 (−2.21)	−0.4*,[e]	–
7-H^{α}		4.05 (14.56)	−1.5*	–
7-$H^{\alpha'}$		4.55 (12.62)	−1.5*	–
7-H^{β}	4	−2.84 (−1.12)	−3.7*	15
7-$H^{\beta'}$		−2.11 (1.18)	−3.7*	18
α-meso-H		0.98	−2.4*	
β-meso-H		5.96	−1.5*	
γ-meso-H		−0.42	−4.9*	
δ-meso-H		5.01	−1.9*	

[a] The hyperfine-shifted spin systems labeled 1–4 correspond to those in text and Fig. 2A.
[b] Chemical shift for the major isomer in ppm from DSS at pH 8.9, 25 °C; the shifts of minor component are given in parentheses.
[c] Slope is $\Delta\delta_{obs}\,\Delta(1/T)$ in ppm · K; * indicates slopes > 1.3×10^3.
[d] At 25 °C, pH 8.9; uncertainty ± 15%.
[e] Although the slope < 1.3×10^3, the chemical shifts showed strong hyperfine shifts.

25 °C-shifts are listed in Tables 1 and 2. Two of the 35 cross peaks involved extremely broad (~ 150 Hz) resonances and could only be observed when the unshifted sine-bell-squared apodization function was used over 256 points in both t1 and t2 dimensions (see Fig. 4A'). Ten strongly temperature-sensitive nonlabile proton peaks were located which did not exhibit COSY, but which displayed NOESY cross peaks or 1D NOEs. These peaks are also labeled with asterisks in Tables 1 and 2. Extension of the variable temperature COSY experiments to ^1H_2O solution revealed strongly temperature-sensitive cross peaks involving four hyperfine-shifted labile protons (slope > $|1.3| \times 10^3$ ppm·K). Three of the hyperfine-shifted labile protons spin coupled to the three different hyperfine-shifted nonlabile protons identified above. Variable temperature NOESY and 1D NOE in ^1H_2O located two strongly hyperfine-shifted labile protons (labeled x, y in Fig. 1A) which did not exhibit COSY peaks. In all, the variable temperature experiments located a total of 54 strongly temperature-dependent signals (labeled with asterisks in Tables 1 and 2), of which 42 exhibited COSY peaks and 12 only exhibited NOEs.

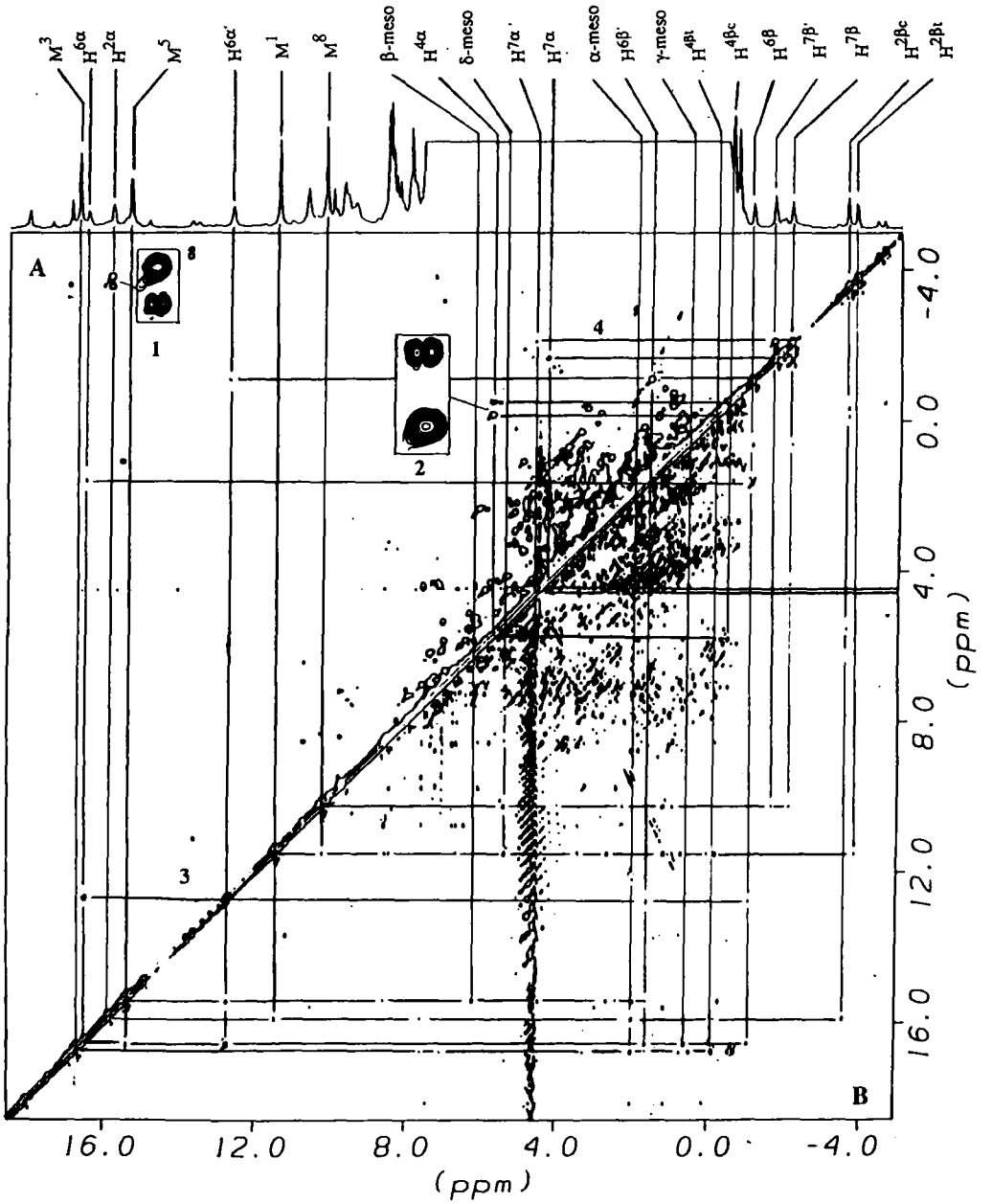

Fig. 2. (A) MCOSY and (B) NOESY (mixing time 50 ms) spectra of *Aplysia* metMbCN in ^2H_2O at 45 °C, pH 8.9, and a repetition rate 2 s^{-1}. Two AMXs (**1** and **2**) and two-CH_2-CH_2-s (**3** and **4**) spin systems are indicated in (A). All the heme proton resonances are labeled in the 1D reference trace.

Identification of side chains

The spin-coupling networks of the 42 strongly hyperfine-shifted protons (4 labile peptide NHs) were defined by a combination of variable temperature COSY and TOCSY spectra over a series

TABLE 2
^{1}H NMR SPECTRAL PARAMETERS FOR HYPERFINE-SHIFTED AMINO-ACID RESIDUES

Residue	Spin system[a]	Peak	δ_{obs}[b] (ppm)	Slope[c] ($\times 10^3$)	T_1[d] (ms)	R_{Fe}[e] (Å)
Phe 43/CD1		$N^{\rho}H$	7.41[f]	0.4		8.9
		$C^{\alpha}H$	4.42 (4.43)	0.1		7.6
		$C^{\beta}H$	3.41 (3.35)	0.7		8.9
		$C^{\beta}H'$	3.91 (3.83)	1.0		8.4
		$C^{\delta}H$	8.87 (8.63)	1.3*		6.4, 7.6
	5	$C^{\epsilon}H$	11.42 (11.01)	3.4*	25	4.3, 6.2
		$C^{\zeta}H$	6.19 (6.41)	−0.8		4.2
Val 63/E7		$N^{\rho}H$	9.60 (9.52)	1.5*		10.0
		$C^{\alpha}H$	7.67 (7.76)	2.5*		7.3
	14	$C^{\beta}H$	4.83 (4.69)	1.9*		8.7
		$C^{\gamma 1}H3$	8.63 (8.41)	4.9*		6.5
		$C^{\gamma 2}H3$	3.50 (3.96)	0.6		8.6
Arg 66/E10		$N^{\rho}H$	8.94	1.0		8.7 (8.8)
		$C^{\alpha}H$	4.26	0.1		8.8 (9.0)
		$C^{\beta}H$	2.27	0.1		7.5 (7.1)
	12	$C^{\beta}H'$	3.26	0.5		8.2 (7.1)
		$C^{\gamma}H$	6.05	3.5*		5.4 (9.4)
		$C^{\gamma}H'$	2.95	1.8*		6.3 (9.6)
		$C^{\delta}H$	3.41	0.4		5.8 (8.8)
		$C^{\delta}H'$	5.80	1.3*		6.5 (8.3)
		$N^{\epsilon}H$	16.20	8.1*	12	3.7 (11.1)
		$N^{\eta}H$	7.19	1.1		
		$N^{\eta}H$	6.80	0.6		
		$N^{\eta}H$	6.44	0.9		
Ile 67/E11		$N^{\rho}H$	9.76 (9.81)	1.4*		7.0
		$C^{\alpha}H$	2.54 (2.61)	−0.6		5.5
		$C^{\beta}H$	3.04 (3.14)	0.5		6.7
	17	$C^{\gamma}H$	9.49 (9.01)	4.7*	21	4.7
		$C^{\gamma}H'$	3.61 (3.81)	1.6*		3.7
		$C^{\gamma}H_3$	−0.35 (−0.28)	0.3		6.6
		$C^{\delta}H_3$	1.30 (1.79)	1.3*		5.0
Phe 91/F4		$N^{\rho}H$	9.12 (9.02)	1.0		10.5
		$C^{\alpha}H$	6.02 (5.94)	1.2*		7.8
	10	$C^{\beta}H$	4.55	0.8		9.2
		$C^{\beta}H'$	4.45	0.6		8.9
		$C^{\delta}H$	8.63	0.4		6.6, 8.1
	6	$C^{\epsilon}H$	8.87 (8.57)	1.9*		4.8, 6.6
		$C^{\zeta}H$	10.73 (10.53)	4.7*	25	4.8
Ala 92/F5		$N^{\rho}H$	10.01 (9.93)	1.1		10.1
	11	$C^{\alpha}H$	6.44 (6.23)	1.4*		8.9
		$C^{\beta}H_3$	2.52 (2.55)	0.7		11.3
His 95/F8		$N^{\rho}H$	11.32 (11.28)	2.3*		6.8
		$C^{\alpha}H$	7.62 (7.99)	1.8*		5.6
	9	$C^{\beta}H$	10.55 (10.38)	4.3*		6.5
		$C^{\beta}H'$	10.72 (10.57)	4.7*		6.1
		$C^{4}H$	18.35	11.0*	~3	3.5
		$C^{2}H$	−2.35	−1.8*	~3	3.2

TABLE 2 (continued)

Residue	Spin system[a]	Peak	δ_{obs}[b] (ppm)	Slope[c] ($\times 10^3$)	T_1[d] (ms)	R_{Fe}[e] (Å)
		N^1H	14.30	2.4*	33	5.1
Val 96/F9		$N^\rho H$	10.77 (10.81)	1.3*		8.8
		$C^\alpha H$	5.21 (5.21)	0.8		9.8
	16	$C^\beta H$	2.91	0.5		10.9
		$C^{\gamma 1}H_3$	1.58	0.2		12.7
		$C^{\gamma 2}H_3$	2.01	0.7		11.3
Phe 98/FG2		$N^\rho H$	7.70[f]	0.5		8.4
		$C^\alpha H$	4.12	0.1		9.5
		$C^\beta H$	2.36 (2.42)	−0.2		7.3
		$C^\beta H'$	2.40 (2.54)	−1.0		6.7
		$C^\delta H$	5.78	−0.9		5.3, 9.1
	8	$C^\varepsilon H$	3.96	−2.9*		5.8, 9.4
		$C^\zeta H$	4.93	−1.9*		8.0
Val 100/FG4		$N^\rho H$	8.50[f]	0.9		8.2
		$C^\alpha H$	3.76 (3.72)	0.6		8.5
	15	$C^\beta H$	3.60 (3.68)	1.5*		6.3
		$C^{\gamma 1}H_3$	0.86 (0.82)	0.5		6.4
		$C^{\gamma 2}H_3$	−0.35 (−0.37)	−0.6		6.1
Phe 105/G5		$N^\rho H$	7.34 (7.24)	0.5		10.1
		$C^\alpha H$	3.22 (3.23)	−0.3		9.1
		$C^\beta H$	2.79 (2.72)	0.1		10.1
		$C^\beta H'$	2.98	0.2		10.0
		$C^\delta H$	7.18 (7.18)	0.3		8.3, 7.9
	7	$C^\varepsilon H$	7.94 (7.81)	1.6*		6.0, 5.6
		$C^\zeta H$	10.54 (10.75)	4.9*	15	4.2
Val 108/G8		$N^\rho H$	6.10 (6.28)	−0.6		10.8
		$C^\alpha H$	2.50 (2.54)	−0.9		11.0
	13	$C^\beta H$	0.94 (0.98)	−0.7		9.8
		$C^{\gamma 1}H_3$	−0.51 (−0.71)	−1.1		9.8
		$C^{\gamma 2}H_3$	−0.96	−1.6*		8.4

[a] The hyperfine-shifted spin systems labeled **5–17** correspond to those described in the text and labeled in Figs. 3 and 4.

[b] Chemical shifts for the major isomer, in ppm from DSS at 25 °C, pH 8.9 (unless noted otherwise); the available minor component shifts are given in parentheses.

[c] Slope is $\Delta\delta_{obs}$; $\Delta(1/T)$ in ppm·K; resonances with slope > ~ 1.1 × 10^3 ppm·K (for labile proton > 1.3 × 10^3 ppm·K) are labeled with an asterisk.

[d] Uncertainty ± 15%.

[e] Distance of protons to heme iron based on *Aplysia* metMbF crystal structure (Bolognesi et al., 1990). The numbers in the parentheses for Arg^{66} (E10) are distances of protons to iron based on ferric *Aplysia* Mb crystal structure (Bolognesi et al. 1989).

[f] Chemical shifts in ppm from DSS at 25 °C, pH 5.3.

of mixing times to detect remote as well as primary connectivities. These 42 resonances factored into 17 spin systems (labeled **1–17** in Figs. 2A, 3A, 3B and 4A) and encompassed an additional 30 resonances with moderate-to-weak temperature sensitivity for a total of 72 signals (note, an amino acid side chain may contain two separate spin systems, e.g., $C^\alpha H$–$C^\beta H_2$ and aromatic ring

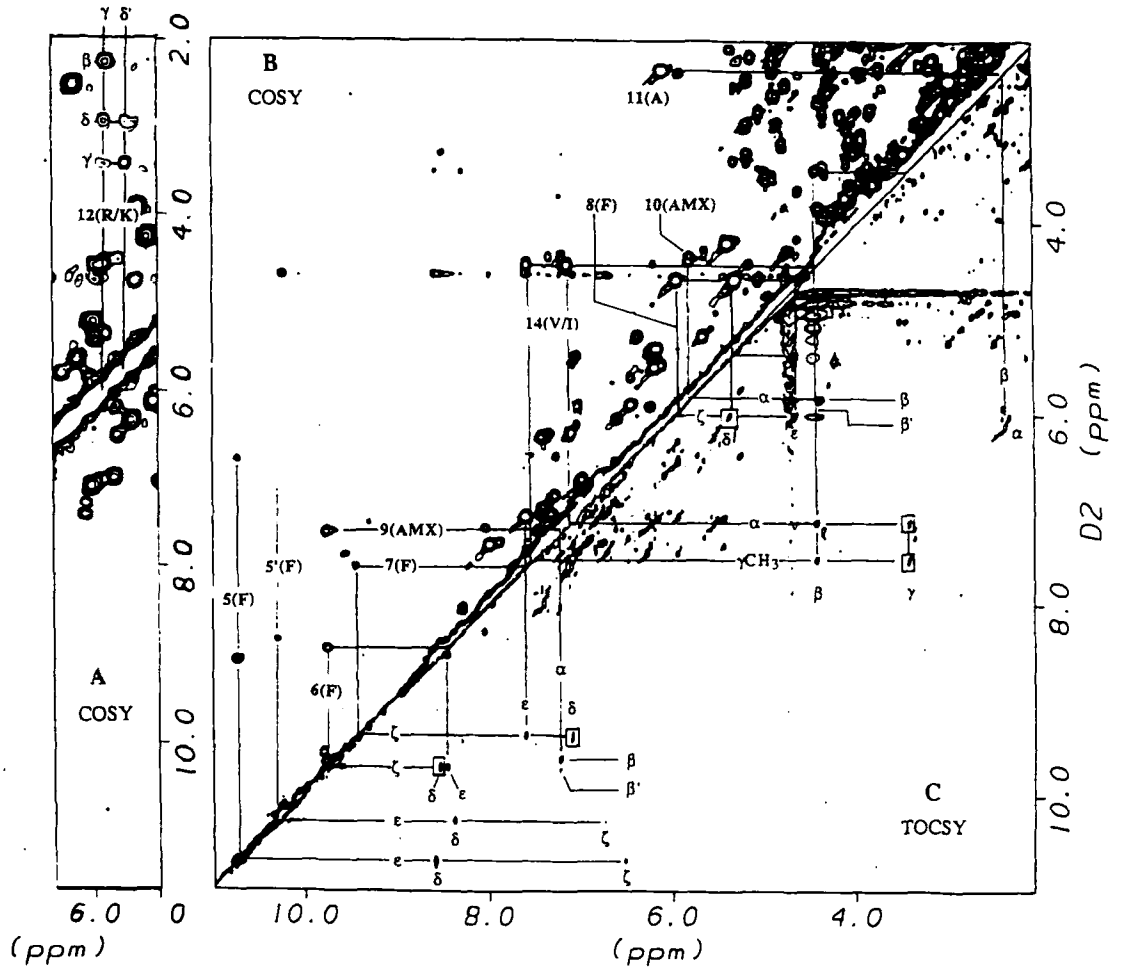

Fig. 3. (A) Low-field portion of MCOSY at 25 °C, (B) MCOSY at 45 °C, and (C) TOCSY spectra (mixing time 30 ms) at 45 °C for *Aplysia* metMbCN in ^2H_2O, pH 8.9, showing **5–8**: Phe ring spin systems; **9–10**: AMX spin systems; **11**: Ala spin system; **12**: part of Arg/Lys spin system showing newly assigned $C^\delta H'$ (refer to Qin et al., 1992); **14**: Val/Ile spin system. The peaks in square boxes in (C) indicate remote cross peaks. The NH-$C^\alpha H$ cross peaks for the spin systems **9–12** and **14** were detected by COSY in ^1H_2O.

spin systems for one Phe). Five of the 30 weakly temperature-sensitive signals were from labile protons. These five NHs, together with the above identified four strongly temperature-sensitive labile protons provided the backbone NH peaks for a total of nine residues (labeled **9–17**), of which some protons showed strong hyperfine shifts. Eight spin systems (labeled **1–8**) did not exhibit any cross peaks to labile protons. The nature of these eight spin systems that excluded labile protons was readily identified. Two AMX systems, **1** and **2**, exhibited coupling patterns diagnostic of heme vinyl groups, while another two involved CH_2-CH_2 fragments, **3** and **4** (Fig. 2A), which must have originated from the heme propionates (see below). The remaining four spin systems, **5–8**, that did not have labile protons had the characteristics of a 'linear' three-spin system (see Figs. 3B and 3C) of which one of the terminal resonances exhibited negligible temperature sensitivity

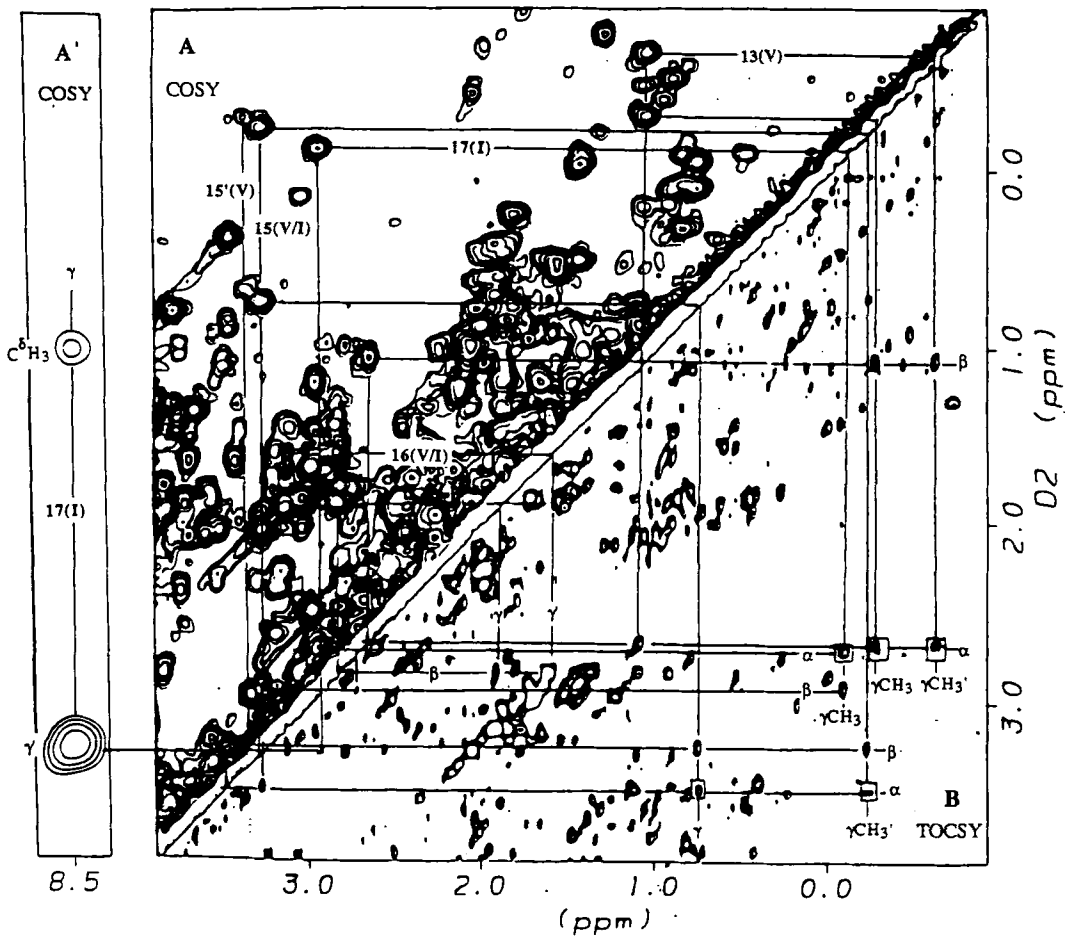

Fig. 4. High-field portions of (A') MCOSY, and (A) MCOSY, and (B) TOCSY (mixing time 30 ms) for *Aplysia* metMbCN in ^2H_2O at 45 °C, pH 8.9, showing **13**: Val; **15–16**: Val/Ile: **17**: Ile spin systems. The peaks in a square box in (B) indicate remote cross peaks. MCOSY data in (A') and (A) were processed differently. 1024 points for (A) and 256 points were apodized by a zero-shifted sine-square window function in both dimensions. The latter emphasized the extremely broad cross peaks. The NH-$C^{\alpha}H$ cross peaks for the spin systems **13** and **15–17** were detected by COSY in ^1H_2O. (The COSY peak between $C^{\alpha}H$ and $C^{\beta}H$ and the remote peaks between $C^{\alpha}H$ and $C^{\gamma}H_3$s for 16 are not shown).

and resonated in the narrow range (~ 6–7 ppm) typical of aromatic side chains. These spin systems could thus be unambiguously assigned to the rapidly reorientating aromatic rings of four Phe residues.

The nine spin systems, each of which encompassed a labile proton, **9–17**, included two with AMX side chains, **9** and **10**, of which **10** showed medium ($C^{\alpha}H$) and strong ($C^{\beta}Hs$) NOESY cross peaks to the $C^{\delta}Hs$ of one of the aromatic side chains (**6**) identified above. Thus **6** and **10** encompassed a complete Phe. The three-spin system including the labile NH, **11**, exhibited shifts only consistent with an Ala (Figs. 3B and 3C). One extended spin system, **12**, which included a complete seven-proton side chain (Fig. 3A), was due to an Arg/Lys previously partly identified (Qin et al., 1992). The previously undetected $C^{\delta}H'$ signal was located in the COSY map at 25° (Fig. 3A).

For one spin system, **13**, identification of a four-spin side chain and detection of two resolved terminal methyl groups uniquely identified a complete Val (Fig. 4). Three four-spin side-chain systems, **14–16**, exhibited the spin connectivity of a complete Val. They could also represent the spin connectivity of an incomplete Ile, even though no additional COSY or TOCSY peaks were observed with severe apodization of the 2D spectra emphasizing broad lines (i.e., apodization over fewer points than collected, such as 256 of 2048 points, in both t1 and t2 dimensions). Hence **14–16** can be described as Val/Ile (Figs. 3 and 4). The remaining six-spin side chain, **17**, was uniquely identified as a Ile (Fig. 4) with a resolved low-field single proton peak ($C^{\gamma}H$) and an upfield methyl peak ($C^{\gamma}H_3$); the spin connectivity of the Ile-CH_2-CH_3 fragment was not observed in COSY until unshifted sine-bell-squared apodization was used over 256 points in both t1 and t2 dimensions. This completely accounted for the 17 spin systems and the encompassing 72 resonances (42 strongly hyperfine-shifted) involved in the spin-coupling networks.

Assignments of heme

The above-described spin systems, two vinyl AMX, **1** and **2**, and the probable propionates CH_2-CH_2, **3** and **4**, exhibited NOESY cross peaks which confirmed their functional group origin and located the remaining heme signals. NOESY cross peaks (Fig. 2B) to two resolved signals with no COSY peaks identified the methyl groups adjacent to the two vinyl groups, 1-CH_3/2-vinyl and 3-CH_3/4-vinyl, but did not differentiate between the two. Similarly, NOESY cross peaks, from the CH_2-CH_2 systems to the other two resolved methyl signals without COSY peaks identified the undifferentiated 8-CH_3/7-propionate and 5-CH_3/6-propionate pairs (Fig. 2B). The NOESY cross peaks between one methyl from each of these pair, however, uniquely identified 1-CH_3 and 8-CH_3 (Fig. 2B), and hence uniquely assigned all pyrrole substituents. The more rapidly relaxed meso-Hs between each pyrrole were identified in the NOESY map by signals with no COSY cross peaks but with NOESY cross peaks to both of the assigned adjacent pyrrole substituents. The 22 complete heme assignments are listed in Table 1. The heme accounted for 14 of 42 strongly hyperfine-shifted signals exhibiting COSY peaks (i.e., 4 of the 17 spin-coupling networks detected) and 8 of 12 strongly hyperfine-shifted signals only exhibiting NOEs. In all, the heme accounted for 22 of the 54 strongly hyperfine-shifted signals. The other 32 signals must have been from amino acids, with 4 only exhibiting NOEs.

Sequential assignment of amino acids in helices

Inspection of the low-field NOESY map in ^1H_2O (Fig. 5B) reveals a series of sequential cross peaks not observed in ^2H_2O which must have arisen from the N_iH:$N_{i+1}H$ connectivities characteristic of α-helices. Three such sequences were clearly identified and encompassed seven ($\mathbf{H}_1$)-, nine ($\mathbf{H}_2$)- and five ($\mathbf{H}_3$)-membered helical segments, of which $\mathbf{H}_1$ and $\mathbf{H}_2$ axhibited large chemical-shift dispersions for both backbone NHs and C^{α}Hs. Each of these NH segments revealed at least two N_iH-$C^{\alpha}H$ cross peaks to hyperfine-shifted residues in the expanded 'fingerprint' region of the ^1H_2O COSY map (Fig. 5A). The helical segment $\mathbf{H}_1$ exhibited the connectivity X_i-Phe $(\mathbf{6,10})_{i+1}$-Ala$(\mathbf{11})_{i+2}$-Y_{i+3}-Z_{i+4}-AMX $(\mathbf{9})_{i+5}$-Ile/Val$(\mathbf{15})_{i+6}$, which the available protein sequence (Tentori et al., 1973) uniquely identifies as residues 90–96. This assigns Phe^{91}, Ala^{92}, part of His^{95}, and dictates that the detected spin system **15** is complete as Val^{96}. The shifts of the main-chain signals of residues 90, 93, and 94 (as well as limited side-chain signals of little interest to the study) are listed in Table 3.

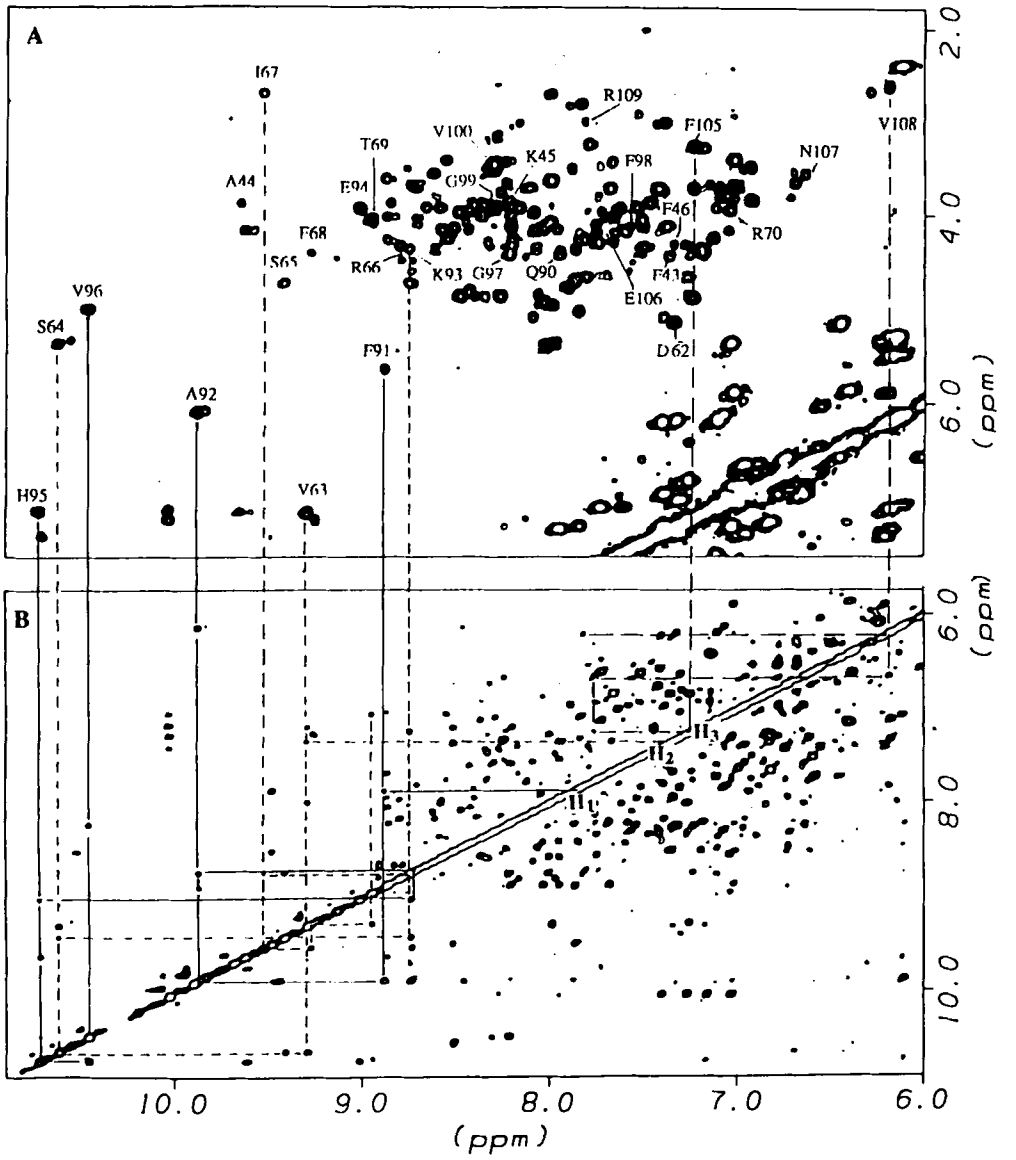

Fig. 5. Finger-print regions of (A) COSY and (B) NOESY spectra (with mixing time 100 ms) in ^1H_2O at 45 °C, pH 5.3. Three helical N_iH-$N_{i+1}H$ NOE sequences ($\mathbf{H}_1$ 90–96, $\mathbf{H}_2$ 62–70, and $\mathbf{H}_3$ 105–109) are indicated. All the assigned N^iH–$C^\alpha H$ COSY peaks from three helical segments and two corners are labeled. The N^iH–$C^\alpha H$ COSY peaks of hyperfine-shifted amino acids from three helical segments are connected by vertical lines to the finger print region of the NOESY map in Fig. 5B to show the wide dispersion of the chemical shift for the backbone NH (over 6 ppm) and $C^\alpha H$ (over 5 ppm) imparted by paramagnetism.

The nine-membered helical segment, $\mathbf{H}_2$, is described by X_j-Ile/Val(**14**)$_{j+1}$-Y_{j+2}-Z_{j+3}-Arg/Lys(**12**)$_{j+4}$-Ile(**17**)$_{j+5}$-X'_{j+6}-Y'_{j+7}-Z'_{j+8}. A portion (j+1 → j+5) of this segment has been described before and shown to identify residues 63–67 (Qin et al., 1992). We extended the segment

TABLE 3
CHEMICAL SHIFT DATA FOR WEAKLY OR NON-HYPERFINE-SHIFTED RESIDUES[a]

Residue	$N^{\rho}H$	$C^{\alpha}H$	$C^{\beta}Hs$	Others
Ala[44]/CD2[b]	9.68	3.87	1.40	
Lys[45]/CD3[b]	8.22	3.79		
Phe[46]/CD4[b]	7.46	3.80	3.23; 3.38	$C^{\delta}H$ 7.44; $C^{\epsilon}H$ 7.99; $C^{\zeta}H$ 7.89
Asp[62]/E6	8.95	5.32		
Ser[64]/E8	10.63	5.41	4.17	
Ser[65]/E9	9.41	4.85		
Phe[68]/E12	9.27	4.50	4.27	
Thr[69]/E13	8.94	4.08	4.4	
Arg[70]/E14	7.04	3.95	1.19; 0.96	$C^{\gamma}H$ 0.74
Gln[90]/F3	8.06	4.60	2.23; 2.41	
Lys[93]/F6	8.68	3.71	2.35; 2.41	$C^{\gamma}H$ 1.74
Glu[94]/F7	9.12	3.90	3.09; 1.38	$C^{\gamma}H$ 1.90
Gly[97]/FG1[b]	8.21	3.87; 4.02		
Gly[99]/FG3[b]	8.48	4.38; 4.44		
Glu[106]/G6[b]	7.77	4.09	2.83; 3.02	
Asn[107]/G7[b]	6.65	3.71	1.80; 2.00	
Arg[109]/G9[b]	7.83	3.02	1.76; 2.38	
Trp[14]/A12[c]				$N^{1}H$ 10.05; $C^{2}H$ 7.14; $C^{4}H$ 7.18 $C^{5}H$ 5.48; $C^{6}H$ 6.12; $C^{7}H$ 7.03
Trp[130]/H8[c]				$N^{1}H$ 10.01; $C^{2}H$ 7.27; $C^{4}H$ 7.04 $C^{5}H$ 5.90; $C^{6}H$ 6.20; $C^{7}H$ 7.43
Phe[29]/B9[c]				$C^{\delta}H$ 5.55; $C^{\epsilon}H$ 6.22; $C^{\zeta}H$7.16
Leu[32]/B13[c]				$C^{\gamma}H$ 0.72; $C^{\delta 1}H_3$ 0.02; $C^{\delta 2}H_3 - 0.74$
Phe[33]/B14[c]				$C^{\delta}H$ 6.60; $C^{\epsilon}H$ 6.66; $C^{\zeta}H$ 6.88

[a] Chemical shift, in ppm from DSS, at pH 8.9, 45 °C.
[b] Chemical shifts (ppm) at pH 5.3, 45 °C.
[c] Assigned based on crystal structure.

from residues 62 to 70 and further confirmed the assignment of this segment by complete spin-system identification of Ile[67]. The Ile/Val **14** obviously corresponded to the complete spin-system for Val[63]. The shifts in the identified main-chain signals from the nonhyperfine-shifted residues on this helix, as well as partial side-chain assignments, are listed in Table 3. The resolved five-membered portion of the remaining helical section, $\mathbf{H_3}$, is described as: $(AMX)_k$-X_{k+1}-Y_{k+2}-Val(**13**)$_{k+3}$-Z_{k+4}. NOESY cross peaks from the above identified hyperfine-shifted aromatic side chain **8** to the $C^{\beta}Hs$ peaks of $(AMX)_k$ dictate that residue k was a Phe, and the sequence thus uniquely identified the segment as comprising residues 105–109, and assigned Phe[105] and Val[108]. The backbone peak shifts from residues 106, 107 and 109 are listed in Table 3. Extension of the backbone assignments of this helix was precluded by degeneracy. The identification of $C^{\alpha}Hs$, $C^{\beta}Hs$ (Fig. 6) for the residues of the three described helical segments showed that not only the helical characteristic N_iH-$N_{i+1}H$, but also the expected C_iH^{β}-$N_{i+1}H$ (strong), C_iH^{α}-$N_{i+3}H$ (weak or medium), and C_iH^{α}-$C_{i+3}H^{\beta}$ (weak or medium) cross peaks were observed. The three helical segments

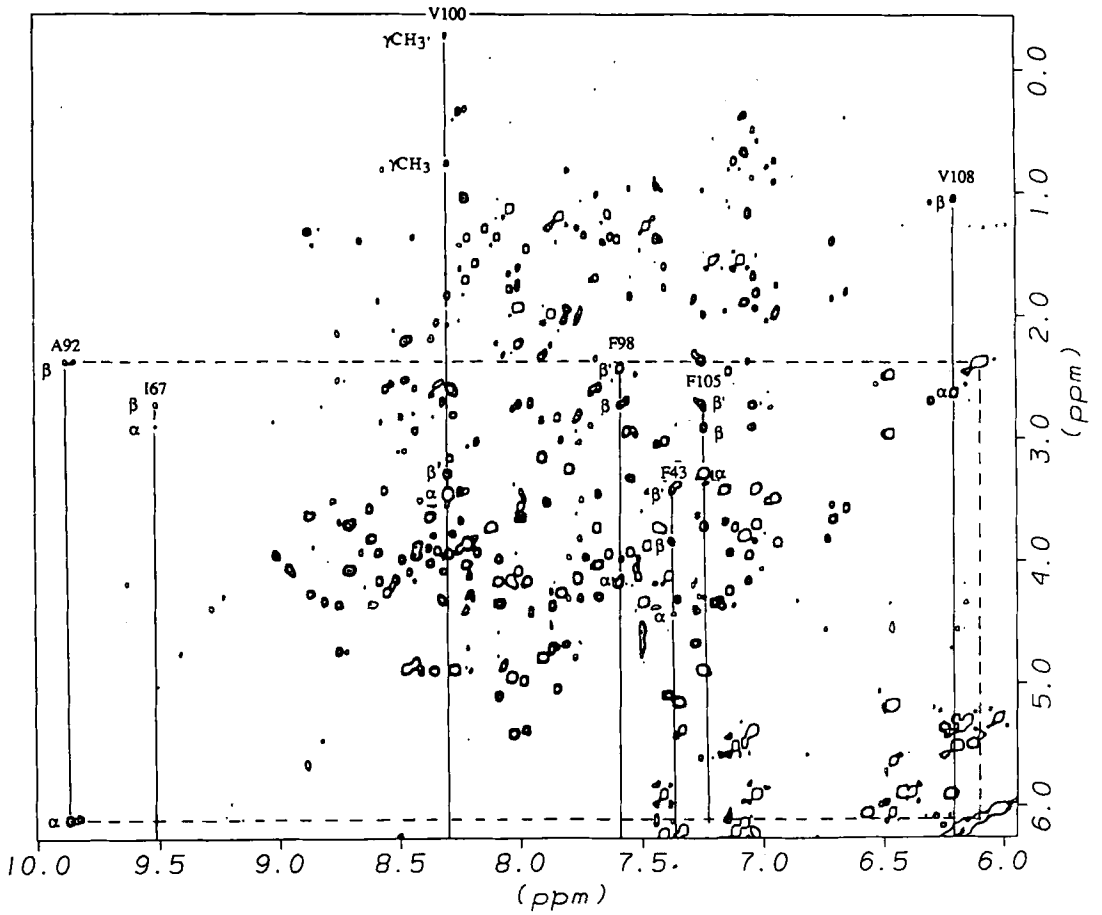

Fig. 6. Finger-print region of the TOCSY (mixing time 38 ms) spectrum in ^1H_2O at 45 °C, pH 5.3, showing NH-C^{α}H-C^{β}H-spin systems of some hyperfine-shifted amino acids. Notice some N^{p}H-C^{γ}H remote peaks were also observed, such as Val ^{100}/FG4 with a mixing time of 38 ms.

accounted for 23 of 42 strongly hyperfine-shifted signals exhibiting COSY peaks (9 of the 17 hyperfine-shifted spin-coupling networks) and 23 of the total 54 strongly hyperfine-shifted signals.

Sequential assignment on loop signals

The N_iH-$N_{i+1}H$ NOEs were disrupted after residue Val^{96} at pH 8.9 but exhibited medium intensity at pH 5.3 and traced the backbone through residues 97–99. TOCSY (Fig. 6) and COSY in ^1H_2O identified an AMX side chain predicted to arise from Phe^{98}; indeed, NOESY cross peaks connected the hyperfine-shifted phenyl group (**7**) to this AMX system. The spin systems of Gly^{97} and Gly^{99} were readily identified. The backbone NHs of residues 99 and 100 resonated very closely to each other, but the NOEs from His^{95}, Val^{96}, and Phe^{98} to the above-defined Ile/Val (**16**) identified the spin system of Val^{100}; TOCSY in ^1H_2O (Fig. 6) mapped the complete spin coupling of Val^{100}. The medium-intensity NOESY cross peak between the Val^{96} $C^{\alpha}H$ and the Val^{100} N_pH and the weak NOESY cross peak between the Val^{96} N_pH and the Val^{100} N_pH confirmed the non-heli-

cal structure for this segment. The observation of medium-intensity N_iH-$N_{i+1}H$ NOEs for this segment at low pH indicated that this corner is not very flexible (Chiu, M., 1992) as compared to segment 43–46 (see below).

The only remaining hyperfine-shifted spin system was the phenyl group **5**. COSY identified an AMX spin system which yielded strong NOESY cross peaks from $C_\beta Hs$ to the $C_\delta Hs$ of ring **5**. The N_iH-$C^\alpha H_i$ cross peak is missing from the pH 8.9 COSY map, but was clearly observed at pH 5.3 (Fig. 5B). The absence of N_iH-$N_{i+1}H$ NOESY cross peaks indicated that this residue was in a flexible nonhelical segment. However, medium-intensity $C^\alpha H_i$- $N_{i+1}H$ cross peaks made it possible to trace the backbone for four residues, with the fourth residue exhibiting an AMX side chain in the COSY map, for which the $C_\beta Hs$ exhibited a NOESY cross peak to a paramagnetically minimally perturbed phenyl ring. Thus the located fragment $Phe(\mathbf{5})_h$ - X_{h+1} - Y_{h+2} - Phe_{h+3} could only be assigned to residues 43(Phe)–46(Phe). The Ala^{44} spin system was also identified and confirmed the loop assignment. The nonhelical segments accounted for the remaining 5 of 42 strongly hyperfine-shifted signals exhibiting COSY peaks (3 of 17 hyperfine-shifted spin-coupling networks) and 5 of the total 54 strongly hyperfine-shifted signals.

Assignment of severely relaxed signals

Four (two nonlabile and two labile) out of a total of 54 strongly hyperfine-shifted signals exhibiting only NOEs remained unassigned. Conversly, two side chains of the above identified 12 hyperfine-shifted amino acid residues were not identified completely, namely, the Arg^{66} guanidyl group (4 or 5 labile protons depending on the state of protonation) and the imidazole group of the axially coordinated His^{95} (two nonlabile and one labile).

The effectively relaxed labile proton signal, y, at 14.3 ppm (Fig. 1A) yielded NOESY cross peaks to both N_pH (label z in Fig. 1A) and $C_\beta Hs$ of the identified His^{95} (mixing time 25 ms; not shown), and hence must have arisen from the labile N_1H of the His^{95} ring. The two very broad ($\sim$ 400 Hz), rapidly relaxing ($T_1 \sim 3$ ms) signals at 18.35 and -2.35 ppm, readily detected in SUPER-WEFT (inset of Fig. 1B), must have arisen from the nonlabile protons, C_2H and C_4H, of the axial His^{95} ring. Neither exhibited NOESY cross peaks even under rapid pulsing conditions, large numbers of scans, and an optimal mixing time ($\sim$ 3 ms). Both signals, however, exhibited 1D steady-state NOEs to the residues assigned above which made it possible to identify them. Saturation of the low-field broad peak in ^2H_2O (Fig. 1C) yielded NOEs to His^{95} $C_\beta Hs$ and Val^{100}. The former contact identified this signal as C_4H. Saturation of the upfield broad signal in ^1H_2O (not shown) yielded a NOE to the above identified N_1H of His^{95}, assigning it to the ring C_2H.

The very broad, rapidly relaxing ($\sim$ 12 ms) labile proton, x, (Fig. 1A) at 16.2 ppm had been previously assigned to the $N_\varepsilon H$ of Arg^{66} (E10), based on its NOEs to $C_\gamma H$ and $C_\delta H$ (Qin et al., 1992), and this was further confirmed by the additional NOE to the newly assigned $C_\delta H'$. The chemical shift of $N_\varepsilon H$ was found to be insensitive to pH (5 to 9), which is consistent with the pK of the guanidyl group of Arg (> 10). Three other weakly temperature-sensitive labile protons from the guanidyl group of Arg^{66} were also located on the basis of the 1D NOE intensity dependence on the composition of the solvent isotope (Qin et al., 1992). This completed the assignment of all 54 strongly hyperfine-shifted signals.

Non-hyperfine-shifted aromatic residues

Here we assigned other aromatic side chains of interest which are remote from the iron and do

not exhibit hyperfine shifts. For these residues, assignments were made on the basis of information deduced from the crystal structures (Bolognesi et al., 1989, 1990; Mattevi et al., 1991). There are only two Trp in the protein sequence, namely at positions 14 and 130. The unique spin systems were identified by a combination of COSY, TOCSY and NOESY cross peaks in both ^1H_2O and ^2H_2O. The specific assignments were made on the basis of an inter-Trp NOE between C_4H of one Trp and C_6H of the Trp, namely that predicted for Trp^{14} and Trp^{130}, respectively. Phe^{28} was assigned by NOESY cross peaks of $C_\varepsilon H$ to heme 2-vinyl and $C_{\gamma 2}H_3$ of Val^{108}, and Phe^{33} was assigned by NOESY cross peaks from $C_\delta Hs$ to Phe^{43} $C_\delta H$ and $C_\varepsilon Hs$ to Val^{63} $C_{\gamma 2}H_3$. The aromatic ring spin-systems for both residues 28 and 33 were identified by COSY and TOCSY cross peaks. Some resonances of Phe residues at positions 28 and 33 were weakly temperature sensitive (Curie slope $< 0.6 \times 10^3$ ppm·k), showing that the residues were paramagnetically minimally perturbed, as expected from the crystal structures. The chemical shifts for the assigned non-hyperfine-shifted residues are listed in Table 3.

Tertiary contacts and paramagnetic relaxation

The protein fold was qualitatively revealed by heme-polypeptide and some interresidue NOESY cross peaks. important contacts between heme and amino acids observed included 1-CH_3 to Ile^{67}, Arg^{70} and Phe^{91}; 2-H_α to Phe^{105} and Val^{108}; 2-H_βs to Ile^{67} and Val^{108}; α-meso-H to Phe^{105} and Val^{108}; 3-CH_3 to Phe^{105} and Val^{108}; 4-H_α to Phe^{43} and Val^{100}; β-meso-H to Val^{100}; 5-CH_3 to Phe^{43}, Phe^{98} and Val^{100}; γ-meso-H to Phe^{98}; 8-CH_3 to Arg^{70} and Phe^{91}; and δ-meso-H to Phe^{91}. Key tertiary interresidue dipolar contact involving the hyperfine-shifted residues observed were for the side chains (on proximal side) from His^{95} to Phe^{91}, Ala^{92}, Phe^{98}, Val^{100} and Phe^{105}, between Phe^{91} and Phe^{105}, and between Phe^{105} and Val^{108}. For the distal side, observed contacts were from Phe^{43} to Val^{63} and Arg^{66}, between Val^{63} and Arg^{66}, and between Ile^{67} and Arg^{66}.

The strongly relaxed protons for which T_1s could be determined (Table 2) allowed a more quantitative determination of structure, tracing the distance to the iron, $R_{(i)}$, as reflected in the differential relaxivity $T_{1j}/T_{ij} = R_{(i)}^6/R_{(j)}^6$ (Cutnell et al., 1981). Using the N_1H of His^{95} with $T_1 = 33$ ms and $R_{Fe-i} = 5.1 \pm 0.1$ Å, as dictated solely by the geometry of a coordinated imidazole ring, the estimated distance to the iron of three signals was determined as Phe^{43}, $R(C_\varepsilon H) \sim 5.0 \pm 0.2$ Å; Phe^{91}, $R(C_\zeta H) = 5.0 \pm 0.2$ Å; and Phe^{105} $R(C_\zeta H) = 4.4 \pm 0.2$ Å.

Minor component

The sequential assignment of hyperfine-shifted residues of the minor component was restricted by its low concentration. However, some COSY peaks for the minor component were readily recognized since they were always paired with much weaker intensities with the corresponding COSY peaks of the major component, such as Phe^{43} and Val^{100} (spin system **5′** in Fig. 3B and spin system **15′** in Fig. 4A, respectively). Saturation of the minor component heme 8-CH_3 (Fig. 1F), previously identified by deuteration (Peyton et al., 1989), gave a NOE pattern very similar to that for saturation of the major isomer heme 5-CH_3 (Peyton et al., 1989). The NOEs from the minor 8-CH_3 to the neighboring amino acids were assigned to minor form Phe^{43}, Phe^{98}, and Val^{100}, which were identified by MCOSY on the basis of their paired COSY peaks and same temperature-sensitivities as the major form. The limited assignments of minor component are listed in Tables 1 and 2.

DISCUSSION

Evaluation of assignment strategy

The use of variable temperature 2D to selectively identify strongly hyperfine-shifted signals can be judged highly successful: 54 signals (22 signals from the heme, 26 nonlabile and 6 labile amino acid peaks) were located, several of them within the intense diamagnetic envelope where their cross peaks at a single temperature would not have given evidence of their origin. The spin correlation experiments were remarkably effective in identifying the complete spin system from hyperfine-shifted residues in spite of lines as broad as 150 Hz and T_1s as short as 15 ms. COSY peaks involving strongly relaxed and broadened resonances were always weak, and hence a combination of a fast repetition rate for COSY with more scans and severe truncation of FIDs by apodizing fewer than the points collected in both the t1 and t2 dimensions (see Fig. 4A') was found to be effective in identifying those broad cross peaks necessary to complete the assignment of side-chain spin systems. These nonlabile side-chain systems were then connected to NH by transferring information to ^1H_2O COSY and TOCSY maps over a range of mixing times. All spin-coupled protons exhibited both COSY and TOCSY cross peaks. However, the broader lines yielded only primary TOCSY connectivity and failed to display any remote cross peaks. This can be attributed directly to the expected effective relaxation in the rotating frame ($T_{1\rho} \sim T_2$) during the longer mixing time. For these resonances, the variable temperature COSY provided the crucial definition of the complete spin system. For any of the less strongly relaxed lines (< 80 Hz), both primary and remote TOCSY peaks were observed.

The 17 spin systems identified by their temperature sensitivity were shown to be the complete spin systems for each fragment, i.e., no COSY cross peaks were lost due to extreme broadening except for the imidazole ring of His^{95}. Thus variable temperature 2D experiments are surprisingly effective in completely defining all but the coordinated residues in the active site. Note that the failure to completely define one (or even several) spin system in the active site, due to paramagnetic relaxation, does not interfere with the complete and unique sequence-specific assignment of all residues giving rise to hyperfine-shifted signals. Such assignments, moreover, were facilitated by the significant improvement in resolution in the fingerprint region due to the hyperfine interaction. The NH dispersion was over 6 ppm, and that for the $C^{\alpha}H$ was over 5 ppm. Degeneracy problems that interfere with further assignments arise as one moves away from the iron center. When strongly relaxed proton signals are resolved, 1D NOEs provide crucial assignments. This was demonstrated by the assignment of proton signals in the His^{95} ring (Fig. 1C). Such 1D NOE experiments will probably continue to serve as limited but crucial adjuncts to complete sequence-specific assignment in paramagnetic proteins. For Arg^{66}, only one guanidyl labile proton exhibited a strong hyperfine shift, and this was assigned to the $N^{\varepsilon}H$, based on NOESY cross peaks to both the $C^{\gamma}Hs$ and $C^{\delta}Hs$ of the same residue. Three other labile protons of the Arg^{66} guanidyl group had been identified previously by 1D NOEs from the $N^{\varepsilon}H$, leaving one labile proton unidentified, since this guanidyl group is expected to be protonated at pH 8.9 ($pK > 10$). The shifts of the three labile protons of the Arg^{66} guanidyl group in addition to $N^{\varepsilon}H$ were weakly temperature sensitive in the crowded 5.8–7.5 ppm window, and the signals were not sufficiently well resolved to allow further stereospecific assignments by either COSY or NOESY.

The 2D methods allowed the complete assignment of the heme protons, including the elusive meso protons under the diamagnetic envelope. These assignments were identical to those resonan-

ces previously assigned by isotopic labeling of the heme moiety (Peyton et al., 1989). The present study demonstrates that isotopic labeling is not necessary if good 2D data can be obtained. Conversely, for minor components present only in ~ 15% of the population, the insufficient intensity of the 2D cross peak precludes the unambigous assignment of the heme signals and hence isotopic labeling is still necessary.

The three stretches of helical segments encompassing residues 62–70, 90–96, and 105–109, and the two nonhelical sections for residues 43–46 and 98–100 correspond to the portions of the protein expected to serve as the active site, on the basis of the Mb fold (Kovac et al., 1976; Lesk et al., 1980), the E-helix (residues 62–70, E6–E14), the F-helix (residues 90–96, F3–F9), the G-helix (residues 105–109, G5–G9), the CD corner (residues 43–46, CD1–CD4) and the FG corner (residues 97–100, FG1–FG4), as clearly demonstrated in the three crystal structures of *Aplysia* Mb (Bolognesi et al., 1989, 1990; Mattevi et al., 1991). The residues of these helices and corners make all of the contacts to the heme and provide most of the residues implicated in the mechanism controlling ligand binding in Mb and Hb. Thus the strategy leads to the assignment of all target residues with hyperfine-shifted protons. One section of the proteins not addressed by our strategy is the B-helix, which, although it has no protons close to the iron, provides three residues, B9, B10 and B14, that line the ligand-binding cavity on the distal side. The reason that these resonances were not addressed in our assignment strategy is that they have only weak hyperfine shifts. We assigned Phe^{28} (B9), Leu^{29} (B10), Phe^{33} (B14) by using crystal coordinates as a guide just to demonstrate that these side chains have their signals minimally shifted from those in a diamagnetic analog (Table 3). Thus the B-helix can be studied by methodology applicable to the diamagnetic system, but was not of explicit interest in this report.

The above strategy, applied with surprising success to *Aplysia* metMbCN, should be able to make significant contributions to the assignment of larger low-spin ferric hemoproteins. The size of the diamagnetic envelope will make the identification of temperature-sensitive cross peaks within the diamagnetic envelope more difficult, but not impossible. Moreover, if the magnetic properties remain unaltered, which appears to be the case for many low-spin ferric hemoproteins, the shift dispersion should facilitate identification of the backbone of the critical proximal and distal helices, and hence permit limited sequence-specific assignments of the active site. Preliminary research suggest that the strategy can be used for the 42-kDa cyanide complex of horseradish peroxidase.

Active-site structural properties of the major isomer

The three crystal structures of *Aplysia* Mb reveal a structurally highly conserved proximal side of the heme (Bolognesi et al., 1989, 1990; Mattevi et al., 1991). The present NOESY cross-peak pattern between the assigned hyperfine-shifted residues and specific portions of the heme, as well as that between side chains of these residues, is consistent with that expected from the crystal structure. The T_1 determination of the distance to the iron for two protons in Phe^{91} (F4) and Phe^{105} (G5) is the same as that obtained from crystal coordinates, providing a more quantitative confirmation for a conserved proximal pocket in *Aplysia* metMbCN.

On the distal side, the three *Aplysia* metMb studies reveal strongly conserved structural elements for all residues except Arg^{66} (E10), which is extended into solution in metMb (Bolognesi et al., 1989), turns into the heme pocket in metMbF (Bolognesi et al., 1990), and is intermediate in metMbN_3 (Mattevi et al., 1991). The remainder of the distal pocket, however, appears to be large-

ly unperturbed. The NOESY contact between the heme and Phe^{43} (CD1), Ile^{67} (E11), between Arg^{66} (E10) and Phe^{43} (CD1), Val^{63} (E7), Ile^{67} (E11), and between Phe^{43} (CD1) and Val^{63} (E7) confirms a similarly conserved portion of the distal pocket. The distances from the iron of all protons of residues of interest are listed in Table 2. For all cases except Arg^{66} (E10), the distances are essentially identical in the various crystal structures (Bolognesi et al., 1989, 1990; Mattevi et al., 1991). Arg^{66} (E10), found with variable orientations in the three crystal structures, is clearly oriented in the heme pocket of metMbCN, as evidenced by the strong paramagnetic relaxation for the labile proton of its terminal guanidyl group, large hyperfine shifts for some side-chain resonances, and NOESY cross peaks to other distal residue protons. The distances to the iron given in Table 2 show that the 'in' orientation of metMbF (R_{Fe} 4–8 Å) could give rise to the observed hyperfine shifts, in contrast to that of the 'out' orientation in metMb (R_{Fe} > 8 Å), where protons are too remote from iron to exhibit strong hyperfine shifts. The NOEs from Arg^{66} (E10) to Val^{63} (E7) and Ile^{67} (E11) and Phe^{43} (CD1) provide additional evidence for the 'in' orientation. A more quantitative description of the distal pocket could be achieved if the observed dipolar shifts are interpreted in terms of the geometric factor. Such an analysis requires the location of the magnetic axis of the iron center and the magnetic anisotropy. Such studies are in progress.

Active-site structure of the minor isomer

The assignments of hyperfine-shifted amino acids of minor components and their very similar chemical shifts (Table 2) show that the heme pocket structure of the minor component is very similar to that for the major component. The similar NOE pattern for Phe^{43} (CD1), Phe^{98} (FG2), and Val^{100} (FG4) protons upon saturation of the major isomer 5-CH_3 and minor isomer 8-CH_3 confirms the earlier proposal that the two isomers differ by a 180°-rotation about the α-γ meso axis (Peyton et al., 1989), as previously established in other myoglobins and hemoglobins (Lecomete et al., 1987; Peyton et al., 1988).

CONCLUSION

All the active-site residues in low-spin cyano-metmyoglobin and monomeric hemoglobin could be identified by conventional sequential assignment NMR methodology. The weakness of some of the cross peaks for efficiently relaxed signals was largely offset by the significant hyperfine shift shown by active-site residues. These hyperfine shifts facilitated the assignments by imparting a strong temperature dependence to the cross peaks, which aids location and identification, and provides an improved spectral dispersion, particularly in the fingerprint region. The strategy of emphasizing cross peaks with strongly temperature-sensitive positions should allow such assignments to be carried out in larger low-spin ferric hemoproteins. The assignment of all residues in contact with the heme revealed a structure fully consistent with that observed by X-ray for other derivatives, except for the distal Arg^{66} (E10), which was turned into the heme pocket, as found only in the metMbF crystal structure.

ACKNOWLEDGEMENTS

The authors are indebted to Professor F. Ascoli and Professor M. Brunori for generously providing the *Aplysia* myoglobin. This research was supported by a grant from the National Insti-

tutes of Health, HL-16087. The NMR instrumentation was purchased, in part, from funds provided by the National Institutes of Health, RR 04975 and the National Science Foundation, BBS-88-04739.

REFERENCES

Antonini, E. and Brunori, M. (1971) *Hemoglobin and Myoglobin in their Reactions with Ligands*, Elsevier North-Holland Publishing Co., Amsterdam.

Bax, A. (1984) *Two-dimentional Nuclear Magnetic Resonance in Liquids*, Delft University Press, D. Reidel Publishing Company, London, UK.

Bax, A., Freeman, R. and Morris, G. (1981) *J. Magn. Reson.*, **42**, 164–168.

Bax, A. and Davis, D.G. (1985) *J. Magn. Reson.*, **65**, 355–360.

Bellelli, A., Foon, R., Ascoli, F. and Brunori, M. (1987) *Biochem. J.*, **246**, 787–789.

Bolognesi, M., Onesti, S., Gatti, G., Coda, A., Ascenzi, P., Giacometti, A. and Brunori, M. (1989) *J. Mol. Biol.*, **205**, 529–544.

Bolognesi, M., Coda, A., Frigerio, F., Gatti, G., Ascenzi, P. and Brunori, M. (1990) *J. Mol. Biol.*, **225**, 621–625.

Braunschweiler, L. and Ernst, R.R. (1983) *J. Magn. Reson.*, **53**, 521–528.

Brunori, M., Ascenzi, P. and Coletta, M. (1986) In *Proceedings of the International Congress on Supermolecules: Biological and Chemical Aspects*, Rome, 9 Nov 1984, Accademia Nazionale dei Lincei, Roma, Italy, pp. 55–73.

Chiu, M. (1992) Ph.D thesis, University of Illinois, Urbana, U.S.A.

Clore, G.M. and Gronenborn, A.M. (1987) *Protein Eng.*, **1**, 275–288.

Clore, G.M. and Gronenborn, A.M. (1989) *CRC Crit. Rev. Biochem. Mol. Biol.*, **24**, 479–564.

Clore, G.M. and Gronenborn, A.M. (1991) *Annu. Rev. Biophys. Biophys. Chem.*, **20**, 29–63.

Cutnell, J.D., La Mar, G.N. and Kong, S.B. (1981) *J. Am. Chem. Soc.*, **103**, 3567–3572.

Davis, D.G. and Bax, A. (1985) *J. Am. Chem. Soc.*, **107**, 2820–2821.

de Ropp, J.S. and La Mar, G.N. (1991) *J. Am. Chem. Soc.*, **113**, 4348–4350.

Dugad, L.B., La Mar, G.N., Banci, L. and Bertini, I. (1990) *Biochemistry*, **29**, 2263–2271.

Emerson, S.D. and La Mar, G.N. (1990a) *Biochemistry*, **29**, 1545–1556.

Emerson, S.D. and La Mar, G.N. (1990b) *Biochemistry*, **29**, 1556–1566.

Ernst, R.R., Bodenhausen, G. and Wokaun, A. (1987) *Principles of Nuclear Magnetic Resonance in One and Two Dimensions*, Clarendon Press, Oxford, UK.

Feng, Y., Roder, H., Englander, S.W., Wand, A.J. and Di Stefano, D.L. (1989) *Biochemistry*, **28**, 195–203.

Giacometti, G.M., Antonini, E. and Brunori, M. (1979) *Biophys. Chem.*, **10**, 119–127.

Janes, S.M., Holtom, G., Ascenzi, P., Brunori, M. and Hochstrasser, R.M. (1987) *Biophys. J.*, **51**, 653–660.

Kovac, A.L., Antonini, E., Brunori, M., Giacometti, G.M. and Tentori, L. (1976) In *Colloquium on Myoglobin* (Eds, Schneck, A.G. and Vanderasseri, C.) Editions de L'University de Bruxelle, Brussels, Belgium, pp. 53–75.

Lecomete, J.T.J., La Mar, G.N., Smit, J.D.J., Winterhalter, K.H., Smith, K.M., Langry, K.C. and Leung, H.-K. (1987) *J. Mol. Biol.*, **197**, 101–110.

Lesk, A.M. and Chothia, C. (1980) *J. Mol. Biol.*, **136**, 225–288.

McLachlan, S.J., La Mar, G.N. and Lee, K.B. (1988) *Biochim. Biophy. Acta.*, **957**, 430–445.

Mattevi, A., Gaffi, G., Coda, A., Rizzi, M., Ascenzi, P., Brunori, M. and Bolognesi, M. (1991) *J. Mol. Recognition*, **4**, 1–6.

Neuhaus, D. and Williamson, M. (1989) *The Nuclear Overhauser Effect in Structural and Conformational Analysis*, VCH Publisher, New York, NY, USA.

Peyton, D.H., La Mar, G.N. and Gersonde, K. (1988) *Biochim. Biophy. Acta.*, **954**, 82–94.

Peyton, D.H., La Mar, G.N., Pande, U., Ascoli, F., Smith, K.M., Pandey, R.K., Parish, D.W., Bolognesi, M. and Brunori, M. (1989) *Biochemistry*, **28**, 4880–4887.

Qin, J., La Mar, G.N., Ascoli, F., Bolognesi, M. and Brunori, M. (1992) *J. Mol. Biol.*, **224**, 891–897.

Rajarathnam, K., La Mar, G.N., Chiu, M. and Sligar, S.G. (1992) *J. Am. Chem. Soc.*, in press.

Rance, M. (1987) *J. Magn. Reson.*, **74**, 557–564.

Satterlee, J. (1985) *Annu. Rep. NMR Spectr.*, **17**, 79–178.

States, D.J., Haberkorn, R.A. and Reuben, D.J. (1982) *J. Magn. Reson.*, **48**, 286–292.

Thanabal, V., de Ropp, J.S. and La Mar, G.N. (1987) *J. Am. Chem. Soc.*, **109**, 265–272.
Thanabal, V. and La Mar, G.N. (1989) *Biochemistry*, **28**, 7038–7044.
Tentori, L., Vivaldi, G., Carla, S., Marinucci, M., Massa, A., Antonini, E. and Brunori, M. (1973) *Int. J. Pept. Prot. Res.*, **5**, 187–200.
Wagner, G. (1990) *Prog. NMR Spectr.*, **22**, 101–139.
Wittenberg, B.A., Brunori, M., Antonini, E., Wittenberg, J.B. and Wyman, J. (1965) *Arch. Biochem. Biophys.*, **111**, 576–579.
Wu, J.Z., La Mar, G.N., Yu, L.P., Lee, K.B., Walker, F.A., Feng, Y.Q. and Sligar, S.G. (1991) *Biochemistry*, **30**, 2156–2165.
Wüthrich, K. (1986) *NMR of Proteins and Nucleic Acids*, Wiley, New York, NY, USA.
Yu, L., La Mar, G.N. and Rajarathnam, K. (1990) *J. Am. Chem. Soc.*, **112**, 9527–9534.